Research Article | Vol. 8, No. 6 | 1 Jun 2018 | OPTICAL MATERIALS EXPRESS 1613
Optical Materials EXPRESS

Demonstration of dimensional control and stabilization of second harmonic electro-optical response in chalcogenide glasses

A. LEPICARD,[1,2] F. ADAMIETZ,[1] V. RODRIGUEZ,[1] K. RICHARDSON,[2] AND M. DUSSAUZE[1,*]

[1]*Université de Bordeaux, Institut des Sciences Moléculaires, UMR 5255 CNRS, 351 Cours de la Libération, 33405 Talence Cedex, France*
[2]*Department of Materials Science and Engineering, College of Optics and Photonics, University of Central Florida, Orlando, FL, USA*
**marc.dussauze@u-bordeaux.fr*

Abstract: Second-order optical susceptibility, $\chi^{(2)}$, has been induced in thermally poled chalcogenide glasses, doped with varying levels of sodium. Using alkali-doped chalcogenide glasses, the second harmonic generation (SHG) capability is retained for over a year whereas in alkali-free glasses it disappears in days. The enhanced stability is attributed to a stabilization of the space charge through structural re-arrangements. Polarization-resolved SHG shows that the induced electric field has components in three spatial directions, all with varying extents of stability. Using structured electrodes, we demonstrate the ability to control the various electric field components' geometry, location and stability to realize a long-lived, nonlinear grating in an alkali-doped chalcogenide glass.

OCIS codes: (160.2750) Glass and other amorphous materials; (160.4330) Nonlinear optical materials; (190.4720) Optical nonlinearities of condensed matter; (160.2100) Electro-optical materials.

References

1. U. Österberg and W. Margulis, "Dye laser pumped by Nd:YAG laser pulses frequency doubled in a glass optical fiber," Opt. Lett. **11**(8), 516–518 (1986).
2. E. M. Vogel, "Glasses as nonlinear photonic materials," J. Am. Ceram. Soc. **72**(5), 719–724 (1989).
3. R. A. Myers, N. Mukherjee, and S. R. Brueck, "Large second-order nonlinearity in poled fused silica," Opt. Lett. **16**(22), 1732–1734 (1991).
4. A. Okada, K. Ishii, K. Mito, and K. Sasaki, "Phase-matched second-harmonic generation in novel corona poled glass waveguides," Appl. Phys. Lett. **60**(23), 2853–2855 (1992).
5. A. Obata, S. Nakamura, Y. Moriyoshi, and K. Yamashita, "Electrical polarization of bioactive glass and assessment of their in vitro apatite deposition," J. Biomed. Mater. Res. A **67**(2), 413–420 (2003).
6. C. R. Mariappan and B. Roling, "Investigation of bioglass-electrode interfaces after thermal poling," Solid State Ion. **179**(19-20), 671–677 (2008).
7. C. R. Mariappan, D. M. Yunos, A. R. Boccaccini, and B. Roling, "Bioactivity of electro-thermally poled bioactive silicate glass," Acta Biomater. **5**(4), 1274–1283 (2009).
8. A. Lepicard, T. Cardinal, E. Fargin, F. Adamietz, V. Rodriguez, K. Richardson, and M. Dussauze, "Surface Reactivity Control of a Borosilicate Glass Using Thermal Poling," J. Phys. Chem. C **119**(40), 22999–23007 (2015).
9. A. Strauß, U. Jauernig, V. Reichel, and H. Bartelt, "Generation of green light in a thermally poled silica fiber by quasi-phase-matched second harmonic generation," Optik (Stuttg.) **121**(5), 490–493 (2010).
10. M. Dussauze, E. Fargin, M. Lahaye, V. Rodriguez, and F. Adamietz, "Large second-harmonic generation of thermally poled sodium borophosphate glasses," Opt. Express **13**(11), 4064–4069 (2005).
11. Y. Nakane, H. Nasu, J. Heo, T. Hashimoto, and K. Kamiya, "Second harmonic generation from thermally poled Ge-S glass system," J. Ceram. Soc. Jpn. **113**(1323), 728–732 (2005).
12. L. A. H. Fleming, D. M. Goldie, and A. Abdolvand, "Imprinting of glass," Opt. Mater. Express **5**(8), 1674–1681 (2015).
13. A. A. Lipovskii, M. Kuittinen, P. Karvinen, K. Leinonen, V. G. Melehin, V. V. Zhurikhina, and Y. P. Svirko, "Electric field imprinting of sub-micron patterns in glass-metal nanocomposites," Nanotechnology **19**(41), 415304 (2008).
14. H. Takagi, S. Miyazawa, M. Takahashi, and R. Maeda, "Electrostatic imprint process for glass," Appl. Phys. Express **1**, 024003 (2008).

#327124 https://doi.org/10.1364/OME.8.001613
Journal © 2018 Received 27 Mar 2018; revised 11 May 2018; accepted 11 May 2018; published 21 May 2018

Optical Materials EXPRESS

15. A. A. Lipovskii, V. V. Rusan, and D. K. Tagantsev, "Imprinting phase/amplitude patterns in glasses with thermal poling," Solid State Ion. **181**(17-18), 849–855 (2010).
16. G. Yang, M. Dussauze, V. Rodriguez, F. Adamietz, N. Marquestaut, K. L. N. Deepak, D. Grojo, O. Uteza, P. Delaporte, T. Cardinal, and E. Fargin, "Large scale micro-structured optical second harmonic generation response imprinted on glass surface by thermal poling," J. Appl. Phys. **118**(4), 043105 (2015).
17. P. G. Kazansky and P. S. J. Russel, "Thermally poled glass: frozen-in electric field or oriented dipoles?" Opt. Commun. **110**(5-6), 611–614 (1994).
18. M. Dussauze, T. Cremoux, F. Adamietz, V. Rodriguez, E. Fargin, G. Yang, and T. Cardinal, "Thermal Poling of Optical Glasses: Mechanisms and Second-Order Optical Properties," Int. J. Appl. Glass Sci. **3**(4), 309–320 (2012).
19. Y. Quiquempois, A. Villeneuve, D. Dam, K. Turcotte, J. Maier, G. Stegeman, and S. Lacroix, "Second-order nonlinear susceptibility in As_2S_3 chalcogenide thin glass films," Electron. Lett. **36**(8), 733–734 (2000).
20. M. Dussauze, X. Zheng, V. Rodriguez, E. Fargin, T. Cardinal, and F. Smektala, "Photosensitivity and second harmonic generation in chalcogenide arsenic sulfide poled glasses," Opt. Mater. Express **2**(1), 45–54 (2012).
21. W. T. Shoulders, J. Novak, M. Dussauze, J. D. Musgraves, and K. Richardson, "Thermal poling behavior and SHG stability in arsenic-germanium sulfide glasses," Opt. Mater. Express **3**(6), 700–710 (2013).
22. M. Guignard, V. Nazabal, F. Smektala, J.-L. Adam, O. Bohnke, C. Duverger, A. Moréac, H. Zeghlache, A. Kudlinski, G. Martinelli, and Y. Quiquempois,, "Chalcogenide glasses based on germanium disulfide for second harmonic generation," Adv. Funct. Mater. **17**(16), 3284–3294 (2007).
23. R. Jing, Y. Guang, Z. Huidan, C. Guorong, K. Tanaka, K. Fujita, S. Murai, and Y. Tsujiie, "Second-harmonic generation in thermally poled chalcohalide glass," Opt. Lett. **31**(23), 3492–3494 (2006).
24. V. Rodriguez and C. Sourisseau, "General Maker-fringe ellipsometric analyses in multilayer nonlinear and linear anisotropic optical media," J. Opt. Soc. Am. B **19**(11), 2650–2664 (2002).
25. V. Rodriguez, "Quantitative determination of linear and second-harmonic generation optical effective responses of achiral or chiral materials in planar structures: Theory and materials," J. Chem. Phys. **128**(6), 064707 (2008).
26. T. Verbiest, K. Clays, and V. Rodriguez, *Second-Order Nonlinear Optical Characterization Techniques: An Introduction* (CRC Press, 2009).
27. D. E. Carlson, K. W. Hang, and G. F. Stockdale, "Ion depletion of glass at a blocking anode - 1, 2," J. Am. Ceram. Soc. **57**, 291–300 (1974).
28. D. A. Kleinman, "Nonlinear Dielectric Polarization in Optical Media," Phys. Rev. **126**(6), 1977–1979 (1962).
29. P. N. Butcher and D. Cotter, *The elements of nonlinear optics* (Cambridge University Press, 1990).
30. L. N. Truong, M. Dussauze, E. Fargin, L. Santos, H. Vigouroux, A. Fargues, F. Adamietz, and V. Rodriguez, "Isotropic octupolar second harmonic generation response in LaBGeO5 glass-ceramic with spherulitic precipitation," Appl. Phys. Lett. **106**(16), 161901 (2015).
31. K. Shimakawa, S. Inami, and S. R. Elliott, "Reversible photoinduced change of photoconductivity in amorphous chalcogenide films," Phys. Rev. B Condens. Matter **42**(18), 11857–11861 (1990).
32. K. Richardson, T. Cardinal, M. Richardson, A. Schulte, and S. Seal, "Engineering Glassy Chalcogenide Materials for Integrated Optics Applications," in *Photo-Induced Metastability in Amorphous Semiconductors,* A. V. Kolobov, ed. (Wiley-VCH Verlag GmbH & Co. KGaA, 2003), pp. 383–405.
33. M. Dussauze, V. Rodriguez, F. Adamietz, G. Yang, F. Bondu, A. Lepicard, M. Chafer, T. Cardinal, and E. Fargin, "Accurate Second Harmonic Generation Microimprinting in Glassy Oxide Materials," Adv. Opt. Mater. **4**(6), 929–935 (2016).

1. Introduction

In photonics, devices increasingly require the combination of components with various optical functionalities such as light sources, guiding elements, detectors and optically active elements serving as beam splitters, modulators, optical switches, and interferometers. Glasses represent the ideal candidate for optical applications as they are low-loss materials, easy to manufacture and are cost-effective compared to single crystals. However, due to their centrosymmetry, their second-order nonlinear susceptibility $\chi^{(2)}$ is null therefore limiting their application in numerous optically active devices relying on second order nonlinear (SONL) optical phenomena. To overcome this limitation, poling techniques which break the centrosymmetry of the medium have been successfully developed [1–4] to enable $\chi^{(2)}$ in glasses. Among these, thermal poling is well documented in the scientific literature and has been used in a variety of applications, from surface reactivity enhancement [5–8], nonlinear optics [9–11], creation of diffractive gratings [12], and as an imprinting process [13–16]. The technique consists of applying a strong DC electric field across a sample heated below its glass transition temperature to dissociate and displace charges inside the glass matrix. The sample is then brought back to room temperature with the outside electric field still applied and only then, is it removed. Charges in the glass matrix are frozen in and a static electric

Optical Materials EXPRESS

field (E_{stat}) is recorded along a longitudinal axis z (where the x-y-plane is defined as parallel to the surface of the glass) therefore breaking the glass' isotropic nature. Kazansky et al. [17] have proposed that the newly available $\chi^{(2)}$ is due to an electro-optical effect, known as Electric Field Induced Second Harmonic (EFISH) which converts the third order nonlinear susceptibility $\chi^{(3)}$ into $\chi^{(2)}$ and which can be written as:

$$\chi^{(2)} = 3\chi^{(3)}E_{stat} \quad (1)$$

As seen in Eq. (1), the newly available $\chi^{(2)}$ is directly linked to the $\chi^{(3)}$ of the base material. Among glasses, chalcogenide glasses (ChGs) possess the highest $\chi^{(3)}$ making them ideal for this technique [18]. In addition, ChG's possess remarkable optical properties including transparency in the mid- and longwave (LW) – IR, large linear refractive indices both of which are readily tailorable through tuning of their composition. Successful poling-induced SHG has been reported in the literature in numerous ChG systems such as the binary As-S [19, 20], ternary As-Ge-S [21], with the best results (as defined by magnitude of induced effect) reported in the germanium antimony sulfide [22] and chalcohalide glasses [23]. The resulting SHG capability realized in these studies however, suffered from several drawbacks as most of the glasses showed low effective $\chi^{(2)}$ with poor temporal stability following poling, when aged at room temperature. The mechanisms of thermal poling of chalcogenide glasses have been discussed in the past but the reason for this low stability has not been explicitly discussed and thus, is not well understood.

Here, we focus on the *magnitude,* the *stability,* and finally *spatial geometrical control* of the induced SONL properties in a Ge-Sb-S chalcogenide glass ($Ge_{22.5}Sb_{10}S_{67.5}$). We demonstrate the positive impact of alkali dopants in the creation of the space charge, through the study of three glasses doped with 0, 1 and 3 mol% of sodium sulfide (Na_2S). We highlight the presence of two main contributions to the SHG signal, one metastable and another stable, with the latter being observed only in alkali-containing glasses. The origin of both contributions to the SHG signal is described and with this knowledge, precise control of the electric field components' geometry, location and stability is realized. By structuring the induced $\chi^{(2)}$ at the micrometric scale we have demonstrated the validity of this induced field control through the creation of nonlinear diffractive gratings. Lastly, we propose a mechanism whereby tailoring the structure of the glass matrix to accommodate and stabilize charge migration, leads to a measurable enhancement of post-poled SHG stability not previously realized in infrared transparent glasses.

2. Methods

All glasses were prepared with high purity elemental Ge, Sb and S (Alfa Aesar, 99.999%) and anhydrous sodium sulfide (purity unspecified) was used to add sodium to the glasses. All raw materials were weighed out in a glove box under nitrogen before being inserted in a quartz ampule. The ampule was then evacuated and sealed using an oxygen-methane torch. The tube was placed in a rocking furnace to ensure better homogeneity. The batch was placed at a homogenization temperature of 850°C overnight. The ampule was then quenched using forced air and the glasses were annealed for 12 hours at T_g-40°C. After annealing, glasses were cut and polished in 1 mm thick disks.

Thermal poling was performed under nitrogen atmosphere to ensure semi-blocking anode conditions. In these conditions, no charges from the atmosphere can be injected inside the glass matrix but mobile species can exit the glass through the electrodes. The glass samples were mechanically pressed between two electrodes (ITO thin film 100 nm thick and 8-12 Ω/sq from Sigma-Aldrich at the anode) and heated from room temperature to 210°C at a rate of 20°C/min. A DC bias of 1300 V was applied between the two electrodes for 30 minutes.

Optical Materials EXPRESS

The sample was then brought back to room temperature and only then was the DC bias removed.

The SHG response of the glasses after thermal poling was measured using the Maker fringe technique, via protocols described elsewhere. [24, 25] The method consists of shining pulsed laser light at the ω frequency upon the sample, and recording the light generated at the 2ω frequency. To perform a complete study of the SHG response, two types of scans were measured: θ-scans and ψ-scans. A θ-scan is performed by rotating the sample therefore changing the angle of incidence θ and leading to a change in effective path length through the sample. This results in the generation of an interference pattern, (Maker fringes), which is recorded as a function of incident angle and which is made of one or multiple fringes depending on the thickness of the poled layer. Here, the input and output light can be independently linearly polarized, either s (vertical), or p (horizontal). Thus, four types of scans, p-p, s-p, p-s or s-s, can be acquired, where the first letter corresponds to the polarization state of the incident beam and the second to the polarization of the collected light. In the case of a ψ-scan, the sample is placed at a fixed incident angle and the SHG intensity is recorded as a function of the polarization angle, ψ, of the incident laser light. The incident beam is initially s-polarized and then goes through a half-wave plate (λ/2) and a fixed quarter wave-plate (λ/4) giving access to all types of polarization of the input laser beam (elliptical, circular left and right circularly polarized, etc.). Careful control of both input and output polarization enables a selective measurement of the various components of the $\chi^{(2)}$ tensor. The incident laser is a 1550 nm nanoseconds laser operating at 30 Hz with a maximum impulsion of 100 μJ during a 20 ns pulse and with a spot size of 100 μm. A simplified representation of the Maker fringe set-up is shown on Fig. 1 along with a reference to position; the bottom row in the figure shows the various states of polarization of the input beam as a function of the angle of the rotating half-wave plate. Further details on this second-order nonlinear characterization technique can be found elsewhere in the literature [26].

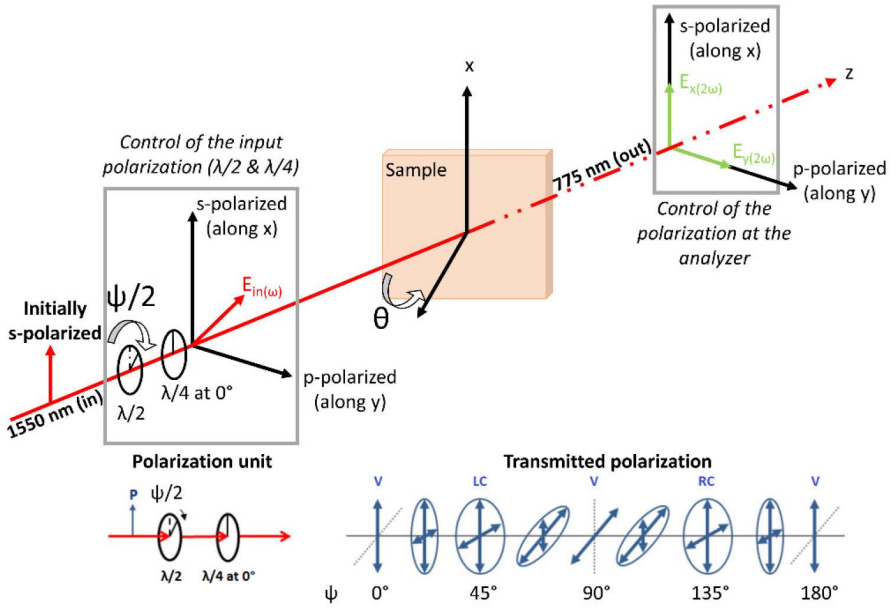

Fig. 1. The Maker fringe set-up with the various scans possibilities shown and the laboratory reference.

Optical Materials EXPRESS

The nonlinear diffraction pattern was measured by placing the sample at normal incidence, the grating facing the incident laser beam. The incident laser was p-polarized and the grating lines were placed perpendicular to this polarization. The detection (a photomultiplier) was scanned behind the sample with an angular step of 0.5° and a 1 mm slit was placed in front of the detection to improve the angular resolution. The scans were then normalized to the square of the incident laser power.

SIMS measurements were performed by Mikhail Klimov at the University of Central Florida on a PHI Adept 1010 Dynamic SIMS system.

3. Results and discussion

3.1 Inducing a stable $\chi^{(2)}$ in thermally poled ChG

Three prepared glasses (doped and undoped) were poled under the same conditions and then analyzed to understand the impact of the alkali on the induced SONL stability. A first difference arises between the sodium-doped and undoped glasses in that during thermal poling, a current up to 0.1 mA/cm^2 was measured in the doped glasses as compared to the undoped glasses where no current is measured under our experimental conditions (limit of detection 0.01 mA). This current reading could be linked to an increase of cationic conductivity in the doped glasses with the increase of sodium content. Secondary Ion Mass Spectrometry (SIMS) was used to probe the depth distribution profile of the various glass' constituents (Ge, Sb, S and Na) on the anodic side of the glass, using a focused ion beam (FIB) to mill through the glass surface. Sodium-free glasses did not exhibit any changes in the distribution of glass constituents after thermal poling as compared to their pre-poled state. Figure 2 shows a typical compositional profile recorded prior to poling of the glass doped with 3 mol% Na_2S as well as a profile recorded on a poled sample from the same glass batch. In the example presented here, a near surface region 6.5 µm thick entirely depleted of sodium is formed after thermal poling (Fig. 2(b)). Similar results (not presented here) were obtained for other doping levels. We observed a small drop in the various component's level once the sodium level returns to the nominal compositions as seen on Fig. 2(b) at depths beyond 6500 nm. This, we believe, is an artifact due to charging of the samples. The SIMS beam parameters were re-adjusted and the level of Ge, Sb and S returned to their original value once milling resumed. These SIMS results demonstrate that upon thermal poling, favored cationic motion of sodium ions takes place to screen the outside electric field. A sodium-depleted layer is therefore formed under the surface, similar to the findings observed previously for oxide glasses [18, 27].

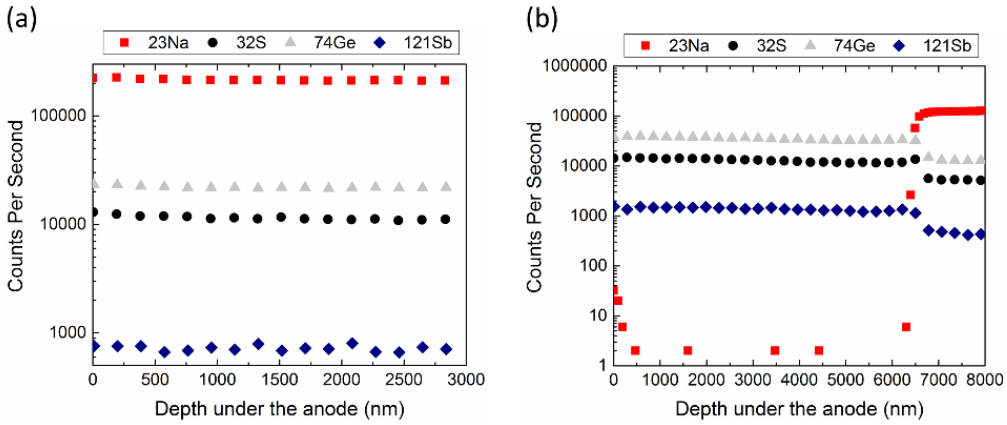

Fig. 2. Secondary Ion Mass Spectroscopy depth profile of the various constituents of glasses doped with 3 mol% Na_2S prior poling (a) and after thermal poling (b). The 0 nm mark corresponds to the surface on the anode side.

Optical Materials EXPRESS

To probe for and quantify the static electric field induced upon thermal poling, a polarization resolved SHG technique, the Maker fringe technique, was used on all glasses on the day of thermal poling. (see section 2 methods for details) The θ-scans measured on the day of thermal poling are shown in Fig. 3. All scans of the various samples presented poor symmetry in their SHG response, especially in the Na-containing glasses. However, if we expect a volumetric electric field homogeneously distributed along the z direction perpendicular to the glass' surface, corresponding to a $C_{\infty v}$ symmetry, the θ scan should be symmetrical and should present one or multiple fringes. As the optical path varies during the θ-scan, any deviation from a symmetric θ-scan pattern indicates that the induced electric field is not so simply distributed at the anode side. In addition, the scans observed immediately after poling sometimes presented a non-zero contribution at normal incidence, a result that is not allowed under the hypothesis of a $C_{\infty v}$ symmetry from a classical EFISH signal. We therefore conclude that additional *in-plane* contributions (along x-y) are at the origin of a SHG signal at normal incidence.

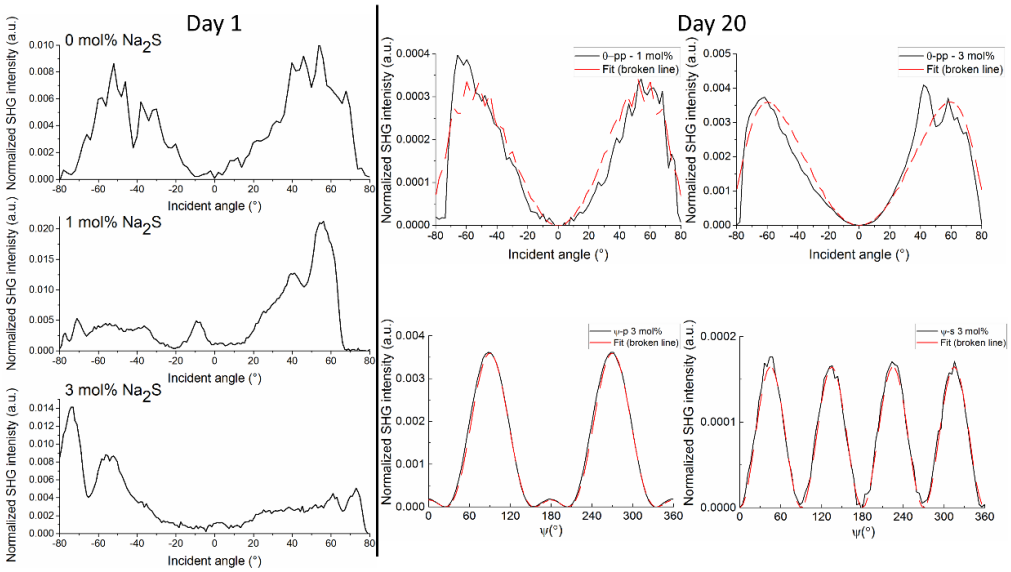

Fig. 3. Left, θ-scans (pp) measured on the day of thermal poling on glasses with various doping level (0, 1 and 3 mol%). Right top row, θ-scans (pp) measured on samples doped with 1 and 3 mol% of Na_2S on Day 20. Right bottom row, ψ-scans (p and s) measured on sample doped at 3 mol%. The red broken lines correspond to the fit of an EFISH process with an electric field induced along z. For comparison reason, the SHG intensities were normalized to the square of the incident laser power.

The evolution of the SHG signal as a function of time after poling was monitored and after a week, no SHG signal could be measured on the alkali-free glasses; this is contrasted by measurements on both alkali-rich glasses, where SHG was still observed. Figure 3 illustrates both θ-scans (top row) and ψ-scans (bottom row) measured on samples doped with 1 mol% and 3 mol% Na_2S, respectively twenty days after thermal poling. After 20 days, the intensity of signal had strongly decreased, down to 4% of the initial magnitude, whereas the contribution at normal incidence was no longer present. More importantly, the signal following this time was symmetrical and matched the classical features expected for a $C_{\infty v}$ symmetry. We then fitted the various scans to the model of an EFISH signal in a thin near-surface layer perpendicular to the plane of the glass surface (plots in red). All scans were fitted at the same time with the same optical parameters, and the thickness of the SHG active layer was fixed to the thickness of the Na-depleted layer as measured by SIMS. A good match was found which validated a longitudinal (along z) EFISH origin of the SHG signal once the

Optical Materials EXPRESS

signal had decayed. The value of the $\chi^{(2)}_{zzz}$ obtained for the glasses doped with 1 and 3 mol% of Na_2S respectively, was 0.1 and 0.3 pm/V at 1550 nm once the SHG had reached a stable plateau. These values are low and indicate that few charges remain frozen in the glass matrix therefore impairing the SHG capability of the glass. Nonetheless, this temporal study clearly proves that the presence of alkali within the glass matrix increases the stability of the SHG signal over time which is a promising first result. All samples were stored in ambient laboratory conditions and re-measured 15 months after thermal poling and the alkali-containing ChGs still retained their SHG capacities on the order of few 10^{-1} pm/V.

3.2 Evidence of a multi-component electric field induced in the thermally poled glasses

We then focused on the origin of the metastable SHG signal to understand the reason behind the enhanced SHG stability in the Na-containing glasses. Two main hypotheses can be made on the origin of this metastable contribution: (i) one due to a structural orientation of polar entities within the glass matrix and (ii) one due to an electro-optical effect induced in the three directions of space (x, y and z) within the sample with a predominant contribution from surface charges (in the x-y plane). On the first days after thermal poling, all measured θ-pp scans were asymmetric but did not show sharp peaks which would be expected in the case of multiple contributing entities. To validate the second hypothesis, ψ-scans at normal incidence were recorded (shown in Fig. 4). The ψ-scans give access to the various components of the $\chi^{(2)}$ tensor and the study of their shape allows one to rationalize on the origin of the signal. When recorded at normal incidence, the ψ-scan only probes the in-plane components of the electric field, i.e. $E_x \neq 0$, $E_y \neq 0$, $E_z = 0$. We make the hypothesis of a gradient of charges along the surface (x,y) which interacts with the isotropic $\chi^{(3)}$ of the glass. At the surface, we therefore assume a space-charge field, E_{stat}, with an arbitrary orientation that can be written in the laboratory frame as:

$$E_{stat} = (aE_x + bE_y) \tag{2}$$

The glass surface is described by a C_S symmetry and, assuming Kleinman symmetry [28], we obtained the following contracted $\chi^{(2)}$ tensor:

$$\begin{bmatrix} d_{11} & d_{12} & d_{13} & 0 & 0 & d_{21} \\ d_{21} & d_{22} & d_{23} & 0 & 0 & d_{12} \\ 0 & 0 & 0 & d_{23} & d_{13} & 0 \end{bmatrix} \tag{3}$$

As the effective $\chi^{(2)}$ is obtained from the interaction between the $\chi^{(3)}$ of an isotropic medium and the electric field E_{stat} frozen in the surface, we can write:

$$d_{11} = a\chi^{(3)}_{xxxx}E_x \tag{4}$$

$$d_{12} = a\chi^{(3)}_{xyyx}E_x + b\chi^{(3)}_{xyyy}E_y \tag{5}$$

$$d_{13} = a\chi^{(3)}_{xzzx}E_x + b\chi^{(3)}_{xzzy}E_y \tag{6}$$

As the glass is an isotropic medium, the terms $\chi^{(3)}_{xyyy}$ and $\chi^{(3)}_{xzzy}$ are null, while the terms $\chi^{(3)}_{xyyx}$ and $\chi^{(3)}_{xzzx}$ are equal [29]. It follows that $d_{12} = d_{13}$. Furthermore, in an isotropic medium, the following relation holds:

$$\chi^{(3)}_{xxxx} = \chi^{(3)}_{xxyy} + \chi^{(3)}_{xyxy} + \chi^{(3)}_{xyyx} \tag{7}$$

Optical Materials EXPRESS

And, as we assume Kleinman symmetry, it naturally follows that $d_{11} = 3d_{12}$. Similarly, we obtain $d_{21} = d_{23}$ and that $d_{22} = 3d_{21}$, which are the classical relationships found in an EFISH effect. The contracted $\chi^{(2)}$ tensor is then simplified to:

$$\begin{bmatrix} d_{11} & d_{12} & d_{12} & 0 & 0 & d_{21} \\ d_{21} & d_{22} & d_{21} & 0 & 0 & d_{12} \\ 0 & 0 & 0 & d_{21} & d_{12} & 0 \end{bmatrix} \quad (8)$$

When measuring a ψ-scan, the first line of the tensor is probed when the analyzer is s-polarized and the second line when the analyzer is p-polarized. The s-polarized scan (in green in Fig. 4) can be fitted to the following expression of the SHG signal and parameters d_{11}, d_{12} and d_{21} returned [30]:

$$I_{\psi s}^{2\omega} \propto \left| P_s^{2\omega}(\psi) \right|^2 = \frac{(E_0^{\omega})^4}{8} \left| {d_{11}}^2 \cos^4(\psi) + {d_{12}}^2 \sin^4(\psi) + 2\left(2\left(d_{21}\right)^2 - d_{11}.d_{12}\right)\sin^2(\psi)\cos^2(\psi) \right| \quad (9)$$

The fit obtained is represented in red in part b of Fig. 4. A similar expression can be written for the ψ-p scan:

$$I_{\psi p}^{2\omega} \propto \left| P_p^{2\omega}(\psi) \right|^2 = \frac{(E_0^{\omega})^4}{8} \left| {d_{21}}^2 \cos^4(\psi) + {d_{22}}^2 \sin^4(\psi) + 2\left(2\left(d_{12}\right)^2 - d_{21}.d_{22}\right)\sin^2(\psi)\cos^2(\psi) \right| \quad (10)$$

As detailed before, for an EFISH effect $d_{22} = 3d_{21}$, and the terms of the ψ-p scan are directly obtained from the parameters returned from the fit of the ψ-s. Assuming an EFISH origin ($d_{22} = 3d_{21}$), the ψ-p scan (in red) was calculated and plotted against the measured data (in black) in part b of Fig. 4. There is a good agreement between the calculated ψ-p scan and that measured on the sample. We therefore conclude that it is possible to describe the measured ψ-scan at normal incidence using a simple model of an electric field induced along the surface of the glass in contact with the anode. The local directionality of the electric field can now be deduced as plotted in a polar plot as shown in part (b) of Fig. 4. This study indicates that the surface currents, responsible for the gradient of charges frozen in the glass, are not controlled and are randomly occurring. The reach of these surface currents is quantified as being on the order of 100 μm as our spot size is 100 μm wide. We can expect that if this study would have been conducted with a 1 mm wide spot, the local directionality of the electric field would have been lost as all frozen charges would be compensated at this scale.

To explain the two-fold origin of the SHG signal in the alkali-doped glasses: (i) a metastable signal which decays rapidly, that can be described by surface charges and (ii) a less intense stable SHG contribution described by a classical volumetric EFISH contribution, we draw a parallel between electro-induced and photo-induced charged defects in chalcogenide glasses as discussed by Shimakawa [31]. We believe that the *metastable* signal is due to what Shimakawa called self-trapped excitons which are unstable charged defects commonly seen in some ChGs which can recombine easily. As chalcogenide glasses are more conductive than their oxide glass counterparts more frequently investigated for thermal poling, we suggest that the metastable in-plane component to the SHG originates predominantly from surface currents at the anode-glass interface resulting in these unstable charged defects. The concentration of such defects and their relaxation are dependent on glass composition. Whereas, the *stable* contribution in our glass is likely due to the creation of

Optical Materials EXPRESS

random pairs which are well-separated, these entities are stabilized through structural re-arrangements. As the stable contribution to the SHG signal is solely along z, we link this stability to the migration of sodium cations under the applied electric field as seen in SIMS. As sodium is displaced to screen the outside electric field, its departure is associated with re-arrangements in the glass network via structural changes where dangling (electron) bonds previously compensated by alkali (Na^+) are now free to re-arrange and reform [32]. These structural re-arrangements allow the stabilization of charges through the creation of well-separated random pairs which are charge compensated by the reformation of initially defective (over- or under-coordinated) bonds. We therefore propose that in both Na-free and Na-containing glasses, the SHG signal measured on the first day after poling is dominated by the *metastable* contribution. The local in-plane components of the electric field are not homogeneously distributed across the surface thereby resulting in asymmetrical θ-scans. Since the EFISH intensity is proportional to the square of the static electric field, we can estimate that the in-plane electric field components are five to seven times greater than the z component. However, as these in-plane contributions are unstable over time, they vanish quickly. The contribution coming from a static electric field along z being stabilized through structural re-arrangements only taking place in the doped glasses, is the only contribution remaining after a week. This is clear evidence that sodium addition to the glass, along with the choice of composition enabling defect pair formation, directly stabilizes the space charge created along z.

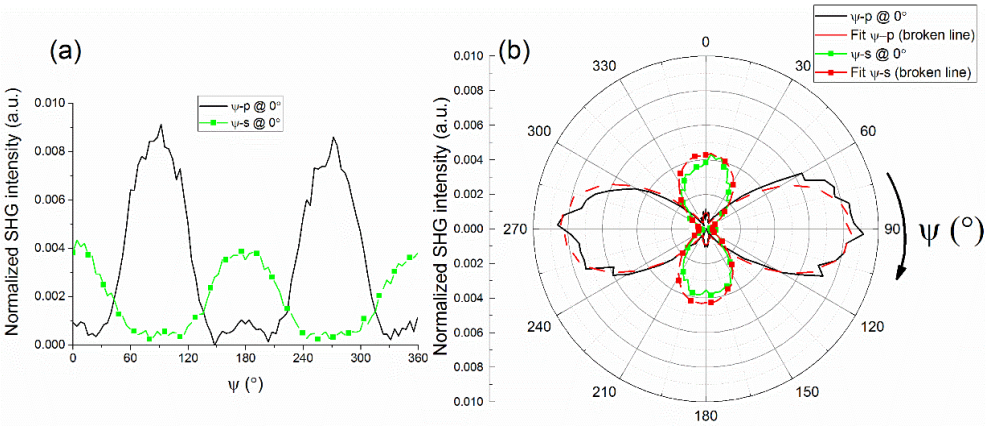

Fig. 4. SHG polarization dependence measured at normal incidence (a) and polar plot of the same Maker fringes with the fit from an electric field induced along x and y (b).

3.3 Towards a micro-structured, stable, in-plane EFISH pattern

The possibility of controlling both in- and out-of-plane induced electric field contributions presents an exciting prospect in microstructural device engineering enabling unique applications in functionality of novel optical components. When controlling in-plane contributions' localization and geometry, our team has shown in niobium borophosphate glasses, that non-linear diffractive gratings could be realized [33]. To confirm this first result in ChGs and to quantify its stability, an ITO-structured electrode was designed using methods described elsewhere [33]. The structured electrode in this example is a 9 mm^2 grating with a pitch of 12 μm. The electrode is made of alternating conductive ITO strips and non-conductive strips (where the ITO electrode material is removed by laser ablation). These non-conductive strips correspond to the lines imprinted on the glass surface, with thickness denoted by *a* while the distance between two neighboring lines is denoted by *b*. The constant *c* denotes the overall period of the grating with $c = a + b$. This peculiar structure allows us to govern the charge density at the glass surface as it favors a field enhancement on the edges of each ITO strip. This configuration also induces charge displacement both in and out of the

Optical Materials EXPRESS

plane of the surface. The structured anode was used during thermal poling of a glass doped with 3 mol% of Na_2S and the electrode's pattern was transferred to the glass' surface with minimum surface relief change (less than 50 nm). The nonlinear diffractive capability of this grating was measured at 1550 nm in transmission mode. The grating was placed at normal incidence, facing the incident laser beam, perpendicular to the incident polarization while the detector was rotated around the sample to record the various Second Harmonic (SH) diffraction peaks. Only the in-plane contributions from the electric field E_y are probed in this configuration. A slit (1 mm wide) was placed in front of the photomultiplier (PM) to improve the angular resolution.

Figure 5(a) and (b) shows the diffraction patterns measured on the day of thermal poling and several months after. Four SH diffractions peaks are observed corresponding to the first and second orders. The third and fourth order SH diffraction peaks are also observed but they exhibit weaker intensities. In addition, one should notice the extinction of the 0^{th} order line. To understand the SH diffraction patterns, a simple model based on an implementation of the in-plane components of the electric field located at the edges of each lines of the electrode pattern is proposed. Such an approach to describe the SH imprinting process is supported by previous observations done by SH microscopy and reported previously by our team [33]. The spatial period of the SH grating is then simply given by the periodicity of the electrode pattern defined earlier by *c*. Two possibilities of the in-plane electric field, E_y, structuring can be considered and are shown in Fig. 5(c). Configuration #1 corresponds to E_y alternating in sign at each edge of the imprinted lines while configuration #2 corresponds to E_y having the same directionality on every line edge (configuration #2 was slightly shifted up for the sake of clarity). However, in both cases, the implementation of the field is maximum exactly at the borders of each ITO strip (line) of the electrode pattern. In our case, *a* (6.8 µm) is larger than *b* (5.2 µm); Fig. 5(d) depicts the theoretical diffraction patterns obtained after Fourier transform of the two configurations presented in Fig. 5(c). As seen on the theoretical diffraction patterns, only configuration #1 gives an extinction of the 0^{th} order line. This model was used to fit the position of the measured diffraction peaks. It is worth pointing out the special case where $a = b$, for which we would have an extinction of all even order lines and be left with the odd diffraction orders. Hence, by playing on the period of the grating, we can tailor the nonlinear diffraction grating to select only specific diffraction orders. Note the field implementation, depending on the poling conditions and the properties of the glass considered, might not be induced exactly at the borders of the line, but can extend further outside the ITO strips of the electrode. To estimate the efficiency of this nonlinear diffraction grating, we recorded a θ-pp scan outside the patterned area and measured the highest intensity of SHG obtained in this region (I_{ppmax}) that we took as our reference value. The intensity of the SH diffraction peaks ($I_n^{th}{}_{peak}$) was then compared to this reference value by taking the ratio of the two ($I_n^{th}{}_{peak} / I_{ppmax}$). Efficiencies of 20% for the first order peaks, 15% for the second order peaks and 2 and 1% respectively, for the third and fourth order peaks were obtained. Overall, these conversion efficiencies represent nearly 80% of the maximum intensity obtained in the unstructured area. The observed decrease of the intensity of the third and fourth order diffraction peaks could be attributed to the limited size of the incident spot (~100 µm) with respect to the period of the pattern (12 µm), behaving as experimental apodization. Such efficiency demonstrates (i) the effectiveness of the imprinting process to control an orientation of the electric field periodically with a high accuracy and (ii) the final optical quality of the device.

Finally, we should discuss the temporal evolution of the diffraction pattern. We observe that the SH diffraction peaks are not symmetric in intensity on the first day (Fig. 5(a)) and tend to disappear over time, only to leave a perfectly symmetrical diffraction pattern (Fig. 5(b)). We believe the mechanisms responsible for these observations are the same as observed with the Maker fringes except that in the present case, the patterning of the electrode adds a strong in-plane component to the electric field. By doing so, the cation migration now takes

Optical Materials EXPRESS

place not only along z but also in the x-y plane of the glass' surface. The use of a structured electrode is thus a way to enhance and control surface current and the spatial scale-length over which they are effective. Some of the charges that are moved in the plane are thus stabilized through structural re-arrangements. These surface currents, which were responsible for the inhomogeneous distribution of the electric field observed previously, are now controlled in term of geometry and location. This nonlinear diffraction grating was re-measured more than a year after (16 months) its creation and still exhibits its SH diffraction capability. This significant, first-ever demonstration of SH stability in poled infrared transparent glasses lends itself to use in the creation of robust bulk and planar optically active devices. The possibility to stabilize the SHG capability of the Na-rich glasses is once more demonstrated as the nonlinear diffractive gratings are still efficient a year after they were realized.

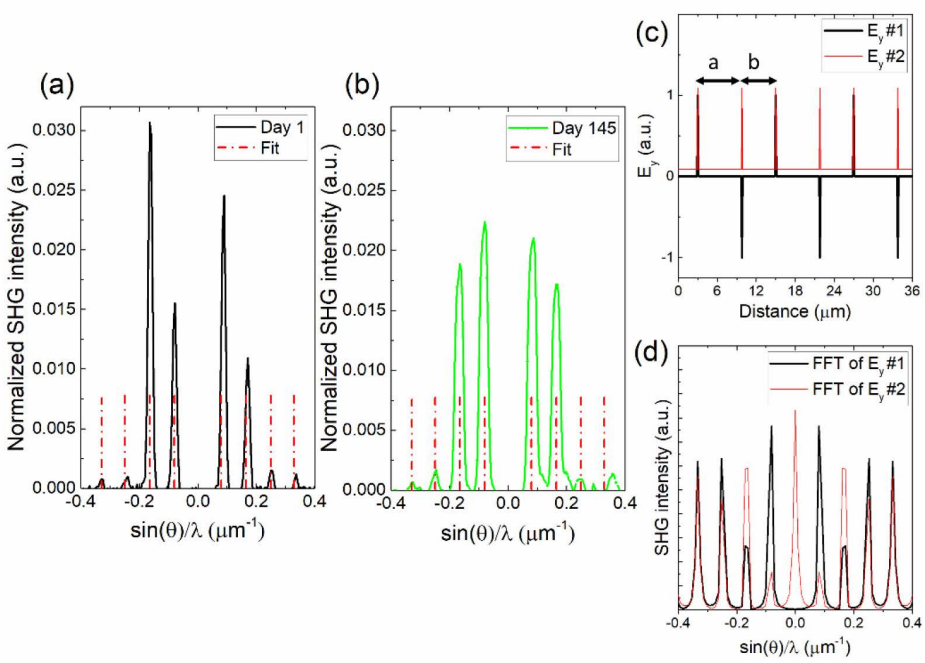

Fig. 5. (a) Nonlinear diffraction patterns in transmission measured on the day of thermal poling and 145 days after poling (b) along with the position of the diffractive peaks (red in a and b) obtained after Fourier transform of the in-plane components of the structured electric field case #1, (c) representation of two envisioned possibilities of electric field structuring, (d) diffraction peaks obtained from both configurations of E_y after Fourier transform.

4. Conclusions

We have experimentally demonstrated and explained the mechanism whereby stable post-poled properties can be realized in chalcogenide glass materials with spatial control that yields unique optical function. We show that upon thermal poling, different types of charges are induced with differing dimensional directions and the type of the resulting charges are dependent on the initial composition of the glass. While the effects of thermal poling in chalcogenide glasses have been previously reported in short-lived experiments on various types of glass, this work for the first time specifically experimentally quantifies the dimensional aspect of the induced charge, the influence on resulting NLO behavior and the

Optical Materials EXPRESS

role compositional choice plays on the stabilization of the post-poled structural reorganization on device formation and stability.

The poling-induced charges are responsible for the creation of a frozen-in electric field inside the glass which we have shown to be at the origin of the glass' SHG capability. This frozen electric field is induced in the three directions of space and we attribute the in-plane components to be the image of inhomogeneous surface current. The charges at the origin of these space charges have been shown to be metastable and can recombine easily resulting in the fast decay of the SHG capability. To stabilize the space charge, we have demonstrated that the addition of alkali to the initial glass results in compositional and structural changes during thermal poling which lead to the creation of stable SONL properties. We attribute the stability to structural rearrangement that takes place in the glass network following the migration of the Na^+ with poling. This has resulted in post-poling stability not previously demonstrated in chalcogenide glass.

Finally, in-plane currents have been shown to be controlled using a structured electrode that enables one to tailor the geometry and distribution of the frozen-in electric field and therefore of the induced $\chi^{(2)}$ in the plane of the glass surface. A specific distribution of the electric field was then designed and imprinted in the glass to successfully demonstrate for the first time, the creation of a nonlinear diffractive grating which retained its capability for over a year after thermal poling

Funding

French National Research Agency (ANR) (LAPHIA ANR-10-IDEX-03-02); Conseil Régional Aquitaine (20121101025); National Science Foundation (#DMR-1308946).

Acknowledgment

This study has been carried out with financial support from the French State, managed by the French National Research Agency (ANR) in the frame of "the Investments for the future" Programme IdEx Bordeaux – LAPHIA (ANR-10-IDEX-03-02), and the French Aquitaine region [Grant 20121101025]. Additionally, the (UCF) authors gratefully acknowledge the partial support to this work by National Science Foundation award #DMR-1308946 and (KR) partial support of the University of Bordeaux's IDeX Visiting Scholar Program.

The authors would like to thank Mikhail Klimov, Research Engineer, at the Materials Characterization Facility (MCF) at the University of Central Florida for conducting all the SIMS measurements.